

1           **A NOVEL PHOX/CD38/MCOLN1/TFEB AXIS**  
2           **IMPORTANT FOR MACROPHAGE ACTIVATION**  
3           **DURING BACTERIAL PHAGOCYTOSIS**

4

5

6

7   Mehran Najibi, Joseph A. Moreau, Havisha H. Honwad, Javier E. Irazoqui\*

8

9

10   Department of Microbiology and Physiological Systems and Program in Innate

11   Immunity, University of Massachusetts Medical School, Worcester MA 01605

12

13

14

15

16   \*Correspondence: [javier.irazoqui@umassmed.edu](mailto:javier.irazoqui@umassmed.edu)

17

18   **Word count:** 9188 including Methods, 7623 without Methods

19   **Keywords:** TFEB, innate immunity, inflammation, infection, phagocyte, transcrip-

20   tion, cytokines, IL-6, IL-1 $\alpha$ , IL-1 $\beta$

## 21 **Abstract**

22 Macrophages are a key and heterogenous class of phagocytic cells of the innate  
23 immune system, which act as sentinels in peripheral tissues and are mobilized  
24 during infection. Macrophage activation in the presence of bacterial cells and  
25 molecules entails specific and complex programs of gene expression. How such  
26 triggers elicit the gene expression programs is incompletely understood. We pre-  
27 viously discovered that transcription factor TFEB is a key contributor to macro-  
28 phage activation during bacterial phagocytosis. However, the mechanism linking  
29 phagocytosis of bacterial cells to TFEB activation remained unknown. In this ar-  
30 ticle, we describe a previously unknown pathway that links phagocytosis with the  
31 activation of TFEB and related transcription factor TFE3 in macrophages. We  
32 find that phagocytosis of bacterial cells causes an NADPH oxidase (PHOX)-  
33 dependent oxidative burst, which activates enzyme CD38 and generates NAADP  
34 in the maturing phagosome. Phago-lysosome fusion brings  $Ca^{2+}$  channel  
35 TRPML1/MCOLN1 in contact with NAADP, causing  $Ca^{2+}$  efflux from the lyso-  
36 some, calcineurin activation, and TFEB nuclear import. This drives TFEB-  
37 dependent expression of important pro-inflammatory cytokines, such as IL-1 $\alpha$ , IL-  
38 1 $\beta$ , and IL-6. Thus, our findings reveal that TFEB activation is a key regulatory  
39 event for the activation of macrophages. These findings have important implica-  
40 tions for infections, cancer, obesity, and atherosclerosis.

## 41 **Introduction**

42 Macrophages are phagocytic cells of the innate immune system, which act as  
43 sentinels in peripheral tissues and are mobilized during infection <sup>1</sup>. Macrophages  
44 are activated in the presence of bacteria, which entails specific programs of gene  
45 expression. Depending on the stimulus and the microenvironment, particularly  
46 the pathogen molecules and cytokines present, macrophages adopt phenotypes  
47 (or “polarize”) along a spectrum, from “classical” activation (a.k.a. M1 polariza-  
48 tion), which is predominantly pro-inflammatory, to “alternative” activation (a.k.a.  
49 M2 polarization), which is predominantly pro-resolution <sup>2</sup>. The activation state of  
50 the macrophage has great functional consequences for health and disease.

51

52 Because transcriptional regulation contributes greatly to the macrophage phe-  
53 notype, understanding the transcription factors that are involved is of paramount  
54 importance. Similarly, it is imperative to fully elucidate the signaling pathways  
55 that regulate such transcription factors under conditions of homeostasis and dis-  
56 ease. Much work has characterized important signaling from the Toll-like recep-  
57 tors (TLRs), which recognize molecules produced by pathogens such as bacteri-  
58 al cell wall components and trigger the activation of transcription factors NF- $\kappa$ B,  
59 IRF3, and AP1 <sup>3</sup>. All three examples of transcription factors are subject to multi-  
60 ple regulatory layers, nuclear-cytoplasmic shuttling being a major mechanism of  
61 regulation.

62

63 We recently identified TFEB as a transcription factor that is important for cyto-  
64 kine and chemokine gene induction in macrophages following bacterial infection  
65 <sup>4</sup>. We found that TFEB resides in the cytosol in resting murine macrophages, but  
66 is imported to the nucleus after short infection with *Staphylococcus aureus* or  
67 *Salmonella Typhimurium* <sup>4,5</sup>. Moreover, cells defective in TFEB expression exhibit  
68 defective induction of important pro-inflammatory cytokines, including TNF- $\alpha$ , IL-  
69 1 $\beta$ , and IL-6 <sup>4</sup>. Subsequent studies confirmed our initial observations, and ex-  
70 tended them by showing that TFE3 is also activated by lipopolysaccharide (LPS),  
71 a cell wall constituent of Gram-negative bacteria <sup>6</sup>. Moreover, an independent  
72 study demonstrated how phagocytosis of opsonized particles triggers TFEB nu-  
73 clear import and the subsequent activation of bactericidal mechanisms in murine  
74 macrophages <sup>7</sup>. Thus, clearly activation of TFEB is an important regulatory event  
75 in macrophage responses to bacterial pathogens. However, the regulatory  
76 mechanisms upstream of TFEB during bacterial infection in macrophages re-  
77 mained unclear.

78

79 We recently reported a novel pathway that is required for TFEB activation dur-  
80 ing bacterial infection in macrophages <sup>5</sup>. In it, phosphatidyl choline-directed  
81 phospholipase C (PC-PLC), which produces diacyl glycerol (DAG), activates pro-  
82 tein kinase D1 (PrKD1) to promote TFEB nuclear import. While in the absence of  
83 this pathway TFEB cannot be activated by infection, its induction is sufficient to  
84 cause TFEB nuclear import. However, the molecular mechanism linking PrKD1  
85 to TFEB remained unknown. Importantly, the link between phagocytosis of bacte-

86 ria and PC-PLC/PrKD1 activation remained unclear.

87

88 In the present article, we describe the discovery of a novel pathway that links  
89 phagocytosis of bacterial cells to TFEB activation and downstream cytokine ex-  
90 pression. Instead of the expected TLR signaling pathways, we found that signal  
91 transduction for TFEB activation requires NADPH oxidase (PHOX) and the pro-  
92 duction of reactive oxygen species (ROS). This event sets in motion the activa-  
93 tion of CD38, which produces NAADP, an activating ligand for lysosomal  $\text{Ca}^{2+}$   
94 export channel TRPML1/MCOLN1. TRPML1/MCOLN1 activation, followed by  
95  $\text{Ca}^{2+}$  export, drives calcineurin, a  $\text{Ca}^{2+}$ -regulated protein phosphatase that  
96 dephosphorylates TFEB on conserved S/T residues critical for TFEB cytosolic  
97 sequestration<sup>8</sup>, thus allowing TFEB nuclear import and downstream gene induc-  
98 tion.

99

100 Because of the broad tissue expression of CD38 and other components of this  
101 pathway<sup>9</sup>, and because several stresses and diseases cause potentially TFEB-  
102 activating ROS production from mitochondria<sup>10-12</sup>, the findings reported here are  
103 likely to have broad implications for the regulation of gene expression down-  
104 stream of TFEB in multiple tissues and physiological conditions, including home-  
105 ostasis and inflammatory diseases.

## 106 Results

### 107 ***Phagocytosis of Gram+ and Gram- bacteria activates TFE3 in macro-*** 108 ***phages***

109 We previously showed that *S. aureus* and *S. Typhimurium* could activate  
110 TFEB in murine macrophages<sup>5</sup>. Since then, several studies have suggested that  
111 TFE3 and TFEB share many features of upstream regulation<sup>13–15</sup>. In addition,  
112 previous work showed that extended incubation with LPS activates TFE3 in mac-  
113 rophages<sup>6</sup>. Therefore, we wondered if TFE3 might also respond to infection by  
114 bacteria. We found that infection with *S. aureus* or *S. Typhimurium* activated  
115 TFE3 with similar kinetics and amplitude as TFEB, measured by its nuclear ac-  
116 cumulation (**Fig. 1A-H** and **S1A-C, F**). Moreover, peptidoglycan (PGN) from *S.*  
117 *aureus* alone was sufficient to induce TFE3 and TFEB nuclear accumulation  
118 (**Fig. 1C, F-H**), suggesting that phagocytosis of large particles was not a re-  
119 quirement. Both *S. aureus* and PGN also induced the formation of lysosomes,  
120 measured with LysoTracker staining (**Fig. 1I-R**). There was a striking correlation  
121 between nuclear accumulation of TFEB and lysosome induction, indicating that  
122 *S. aureus*- or PGN-induced TFEB activation was biologically relevant.

123

124 *Salmonella* infection produced a more nuanced response. As we previously  
125 showed, live and dead *Salmonella* differed in their ability to induce TFEB activa-  
126 tion<sup>5</sup>. While live *Salmonella* induced rapid activation of TFEB and TFE3, dead  
127 *Salmonella* did so much more slowly (**Fig. S1A-D, F, G**). Interestingly, the kinet-

128 ics of TFEB and TFE3 activation by dead *Salmonella* resembled that of LPS,  
129 suggesting that they might trigger TFEB/3 activation through a similar sensing  
130 mechanism (**Fig. S1E, H**). In contrast to *S. aureus*, *Salmonella* did not induce the  
131 accumulation of lysosomes, but rather decreased it below baseline (**Fig. S2A**).  
132 LPS induced lysosomal accumulation, as PGN did (**Fig. S2C**). Thus, we suspect  
133 that *Salmonella* possesses a mechanism to inhibit lysosomal biogenesis down-  
134 stream of TFEB/3. This is consistent with previous results showing lysosomal in-  
135 hibition by *Salmonella*<sup>16,17</sup>.

136

137 The overall conclusion of these observations is that bacterial infection and  
138 bacterial ligand stimulation of murine macrophages causes biologically significant  
139 TFEB and TFE3 activation. However, the functional consequences of bacterially-  
140 induced TFEB and TFE3 nuclear import were unclear.

141

142 ***TFEB and TFE3 are key contributors to the macrophage transcriptional***  
143 ***response to infection***

144 To better understand the functional consequences of TFEB and TFE3 activa-  
145 tion during bacterial infection, we performed RNAseq of a RAW264.7 murine  
146 macrophage cell line harboring deletions in *Tfeb* and *Tfe3*. We detected induction  
147 of 1,022 genes after 3 h of *S. aureus* infection in wild type macrophages (**Table**  
148 **S1, Fig. 2A**). Compared to wild type cells, *Tfeb*<sup>-/-</sup> *Tfe3*<sup>-/-</sup> (double knockout, or  
149 dKO) cells exhibited a drastically altered transcription profile (**Fig. 2A, C**). Over-

150 all, about two-thirds of *S. aureus*-induced genes in wild type macrophages were  
151 not induced in dKO cells (**Fig. 2D**), indicating that a large majority of the tran-  
152 scriptional response to *S. aureus* was TFEB/3-dependent. In addition, while wild  
153 type macrophages induced *Ccl5*, *Nos2*, *Ptgs2*, and *Tnf*, indicating a classically-  
154 activated state, dKO cells were completely defective in their induction (**Fig. 2B**).  
155 This revealed that macrophage polarization to the classically activated state, or  
156 M1, requires TFEB and/or TFE3.

157

158 A large group of innate immunity genes exhibited decreased expression in  
159 dKO cells (**Fig. 2C**). Noteworthy examples included TLR genes *Tlr6*, *Tlr9*, and  
160 *Tlr13*, NF- $\kappa$ B transcription factor genes *Nfkb2* and *Rel*, NF- $\kappa$ B inhibitor genes  
161 *Nfkbib* and *Nfkbie*, and NLR genes *Nod1*, *Nod2*, *Naip2*, and *Naip5*. In addition,  
162 several cytokine genes exhibited defective expression, including *Tnf*, *Il1b*, *Il6*,  
163 *Ifnb1*, *Tgfb1*, *Csf1*, *Csf2*, and *Csf3*, and various interleukins (e.g. *Il23a*, *Il27*, and  
164 *Il33*), as well as chemokines and chemokine receptors such as *Ccl3*, *Ccl6*, *Ccl7*,  
165 *Ccl12*, *Ccl17*, *Ccl22*, *Cxcl3*, *Cxcl10*, *Cxcl11*, *Ccr2*, *Cx3cr1*, and signaling compo-  
166 nents such as *Ripk2*, *Jak3*, *Stat1*, *Stat2*, and *Stat5a*. Moreover, several autophagy  
167 and lysosomal genes showed lower expression: Cathepsins (lysosomal prote-  
168 ases *Ctsa*, *Ctsd*, *Ctse*, *Ctsz*), *Sqstm1*, *Mcoln1* and *Mcoln2*, *Atg7*, *Atg13*, *Irgm1*  
169 and *Irgm2*, and *Map1lc3a* (LC3). Finally, expression of ER unfolded protein re-  
170 sponse transcription factor gene *Xbp1* and necroptosis effector gene *Mik1* were  
171 also reduced in dKO macrophages. These results strongly suggest that TFEB/3  
172 are important for many key functions of macrophages, including pathogen recog-



173 nition, pro-inflammatory signaling, secretion of chemotactic signals, and autophagy/lysosomal clearance.

175

176 More systematically, analysis of over-represented Reactome pathways<sup>18</sup> revealed that the top affected categories were “Cytokine Signaling in Immune System”, “Signaling by Interleukins”, and “Innate Immune System”. Other significant categories affected were “Interferon signaling”, “ER-Phagosome Pathway”, and various TLR pathways (**Fig. 2E**). Consistent with the transcriptome measurements, we observed robust secretion of IL-6 in *S. aureus*-infected wild type murine macrophages, which was abrogated by deletion of *Tfeb* alone (**Fig. 2F, H**). Wild type cells also secreted more IL-1 $\beta$  and TNF- $\alpha$  than *Tfeb* <sup>$\Delta$ LysM</sup> macrophages, even though in this case the secreted levels were noisier than IL-6 (**Fig. 2H, J**). IL-1 $\alpha$  exhibited a similar trend to IL-1 $\beta$  (**Fig. 2G**). Lactate dehydrogenase (LDH) release assays ruled out that these differences were due to cytotoxicity (**Fig. 2K**). Together, these observations provide strong evidence that TFEB/3 are essential for the macrophage transcriptional response to *S. aureus* infection, for macrophage polarization and function, and for the production of pro-inflammatory cytokines and chemokines. They also suggest that *Tfeb* deletion alone is sufficient to confer a defect in cytokine production, consistent with previous results<sup>6</sup>. Therefore, nuclear translocation of TFEB and TFE3 is a key regulatory event for the macrophage response to infection. However, the signaling events upstream of TFEB/3 activation remained undefined.

195

196 ***Bacterial infection activates TFEB and TFE3 independently of TLR sig-***  
197 ***naling***

198 Because TLRs constitute a major mechanism of innate recognition of bacterial  
199 ligands, we investigated the roles of TLR signaling in TFEB activation by bacteri-  
200 al cells and ligands. MyD88 is a protein adaptor that is important for signaling  
201 from TLR2/6 and TLR4, which detect PGN and LPS, respectively <sup>19</sup>. TRIF is an  
202 adaptor that is also important for signaling from endosomal TLR4 <sup>20</sup>. Together,  
203 MyD88 and TRIF are essential for TLR signaling. Therefore, we examined TFEB  
204 activation in murine macrophages lacking both MyD88 and TRIF.

205

206 Much to our surprise, after infection with *S. aureus* and treatment with PGN  
207 *Myd88<sup>-/-</sup> Trif<sup>-/-</sup>* macrophages exhibited the same levels of TFEB activation as wild  
208 type cells (**Fig. 3**). Similarly, after infection with *Salmonella* or treatment with  
209 TLR4 agonists LPS or MPLA we observed no difference between *Myd88<sup>-/-</sup> Trif<sup>-/-</sup>*  
210 and wild type macrophages (**Fig. S2**). These results suggested that TLR signal-  
211 ing is dispensable for TFEB activation by bacterial cells and ligands, regardless  
212 of cell wall structure.

213

214 To test this conclusion further, we examined TFEB activation in macrophages  
215 deficient for TLR2 and TLR4 (**Fig. S3A, B**). After infection with *S. aureus* and  
216 PGN or Pam3Csk4 treatment, *Tlr2<sup>-/-</sup>* macrophages exhibited the same activation  
217 of TFEB as wild type cells (**Fig. S3C-L**). Likewise, after infection with live *Salmo-*

218 *nella* or treatment with LPS, TFEB activation in *Tlr4*<sup>-/-</sup> and wild type macrophages  
219 was indistinguishable; MPLA still activated TFEB in *Tlr4*<sup>-/-</sup> cells, albeit more weak-  
220 ly (**Fig. S3M-X**). Together, these results indicated that bacterial cells and ligands  
221 activate TFEB by a TLR-independent pathway.

222

### 223 ***Bacterial activation of TFE3 requires the PC-PLC/PrKD1 pathway***

224 Given this lack of relevance of TLR signaling, we sought alternative mecha-  
225 nisms of TFE3 activation. We previously showed that TFEB activation in macro-  
226 phages infected with *S. aureus* or *Salmonella* required the activity of a pathway  
227 upstream of PrKD1<sup>5</sup>. We found that prior inhibition of PC-PLC with D609 or of  
228 PrKD with kb-NB142-70 completely abrogated TFE3 activation by *Salmonella*,  
229 LPS, and *S. aureus*, similar to TFEB (**Fig. S4A-N**). Furthermore, we observed  
230 strong TFE3 activation by the DAG analog PMA, which was prevented by PrKD  
231 inhibition (**Fig. S4O, P**). Together, these data indicate that the PC-PLC/PrKD1  
232 pathway is necessary and sufficient for TFE3 activation during infection in mac-  
233 rophages, as we previously showed for TFEB. However, the connection between  
234 PrKD1 and TFEB (or TFE3) nuclear import remained unclear. More importantly,  
235 the mechanism connecting phagocytosis of bacteria to TFEB/3 activation re-  
236 mained unknown. Therefore, we decided to examine regulatory events more  
237 proximal to TFEB.

238

239 ***Bacterial activation of TFEB requires the TRPML1/MCOLN1 – Ca<sup>2+</sup> –***  
240 ***calcineurin pathway***

241 The Ca<sup>2+</sup>-dependent protein phosphatase calcineurin was recently shown to  
242 be principally responsible for TFEB nuclear import induced by starvation in HeLa,  
243 HEK293, and human fibroblasts, as well as mouse muscle and MEFs. Such ef-  
244 fect was mediated by its dephosphorylation of mTORC1 target sites in TFEB <sup>21</sup>.  
245 However, the role of calcineurin in TFEB control in infected macrophages has not  
246 been tested before. Therefore, we evaluated TFEB activation in infected macro-  
247 phages lacking calcineurin function. Prior incubation with Ca<sup>2+</sup>-chelating agent  
248 BAPTA prevented TFEB activation by *S. aureus* (**Fig. 4A-E**), suggesting that in-  
249 tracellular Ca<sup>2+</sup> is important. Moreover, prior treatment with calcineurin inhibitor  
250 FK506 prevented *S. aureus*-triggered TFEB activation even more effectively (**Fig.**  
251 **4D, E**), suggesting that calcineurin activity was required. Furthermore, siRNA-  
252 mediated silencing of genes *Ppp3cb*, which encodes calcineurin catalytic subunit  
253  $\beta$ , or *Ppp3r1*, which encodes calcineurin regulatory subunit B $\alpha$ , abrogated TFEB  
254 activation by *S. aureus* (**Fig. 4F-L**). These experiments indicate that calcineurin  
255 is required for TFEB activation during *S. aureus* phagocytosis. We found similar  
256 results during infection with *Salmonella* (**Fig. S5A-L**), indicating that calcineurin is  
257 a general requirement for TFEB activation during infection of macrophages. Fur-  
258 thermore, the Ca<sup>2+</sup> ionophore ionomycin was sufficient to trigger TFEB nuclear  
259 import in uninfected macrophages (**Fig. 4M-O**). Thus, activation of calcineurin is  
260 necessary and sufficient for TFEB nuclear import in macrophages during infec-  
261 tion with *S. aureus* or *Salmonella*.

262

263 Previous studies have identified TRPML1/MCOLN1 as a major  $\text{Ca}^{2+}$  export  
264 channel in lysosomes<sup>22</sup>. Furthermore, TRPML1/MCOLN1 was shown to function  
265 upstream of calcineurin for TFEB activation in several human and mouse cell  
266 types during nutrient starvation, and TRPML1/MCOLN1 was required for TFEB  
267 activation by FcγR during phagocytosis of opsonized beads in murine macro-  
268 phages<sup>7,21</sup>. In our hands, silencing of *Mcoln1* completely prevented TFEB activa-  
269 tion and lysosome induction by *S. aureus* (**Fig. 4P-T**) and *Salmonella* (**Fig. S5M-**  
270 **Q**). Conversely, treatment of uninfected macrophages with TRPML1/MCOLN1  
271 agonist ML-SA1<sup>23</sup> resulted in strong TFEB nuclear import (**Fig. 4U-W**). Thus, in  
272 macrophages TRPML1/MCOLN1 is necessary and sufficient for TFEB activation  
273 during infection. Together, these results suggested that the TRPML1/MCOLN1-  
274 calcineurin-TFEB pathway is functional in macrophages, and is necessary and  
275 sufficient for TFEB nuclear import during infection. However, the mechanism of  
276 TRPML1/MCOLN1 activation during infection remained unknown.

277

### 278 ***CD38 functions upstream of TRPML1/MCOLN1 for TFEB activation***

279 Because of its relevance to lysosomal storage disorders, in particular  
280 mucopolipidosis Type IV, the regulation of TRPML1/MCOLN1 is of great interest<sup>22</sup>.  
281 Recently, it was reported that nicotinic acid adenine dinucleotide phosphate  
282 (NAADP) can function as a TRPML1/MCOLN1 ligand to induce lysosomal  $\text{Ca}^{2+}$   
283 export in several cell types<sup>24,25</sup>. Therefore, we investigated whether NAADP  
284 might function to induce TFEB activation downstream of MCOLN1 during infec-

285 tion in macrophages.

286

287 Prior treatment with the potent NAADP antagonist Ned-19<sup>26</sup> rendered macro-  
288 phages unable to translocate TFEB into the nucleus during infection with *S.*  
289 *aureus* (**Fig. 5A-C, F**). Likewise, treatment with kuromanin or apigenin, which in-  
290 hibit the NAADP-synthesizing enzyme CD38<sup>27,28</sup>, also prevented TFEB activa-  
291 tion by *S. aureus* (**Fig. 5D-F**). We obtained essentially the same results with  
292 *Salmonella* (**Fig. S6A-F**). Moreover, silencing of *Cd38* prevented TFEB activation  
293 by *S. aureus* (**Fig. 5G-J**). Together, these data showed that CD38 and NAADP  
294 were required for TFEB activation during infection. Conversely, treatment of mac-  
295 rophages with the NAADP analog NAADP-AM<sup>29</sup> resulted in strong induction of  
296 TFEB nuclear import (**Fig. 5K, L, N**). Together, these observations showed that  
297 CD38 and its product NAADP are necessary and sufficient for TFEB activation by  
298 *S. aureus* in macrophages. In contrast, NAADP-AM-induced TFEB activation was  
299 abrogated by silencing *Mcoln1* (**Fig. 5M, N**), suggesting that CD38 and NAADP  
300 require TRPML1/MCOLN1 to induce TFEB translocation, consistent with their  
301 proposed roles upstream of TRPML1/MCOLN1.

302

303 Immunofluorescence in untreated macrophages showed that CD38 localized  
304 principally to the plasma membrane, as previously shown in several human lym-  
305 phocyte cell types<sup>30,31</sup>. In contrast, *S. aureus*-infected macrophages exhibited  
306 intracellular staining in what appeared to be cytosolic vesicles (**Fig. 5O, P**). Such  
307 vesicles are presumably phagosomes<sup>32</sup>. We also noticed increased staining in

308 infected cells compared to baseline. To further examine this, we performed  
309 immunoblots. In wild type macrophages, we observed a slight increase in CD38  
310 expression, albeit of a smaller molecular weight form (45 kDa v 64 kDa), in in-  
311 fected cells compared to control (**Fig. 5Q**). This increased expression occurred in  
312 *Tfeb*<sup>-/-</sup> cells as well (**Fig. 5Q**). Together, these observations suggested that infec-  
313 tion caused the relocalization of CD38 to endomembranes, its increased expres-  
314 sion, and its presumed proteolytic conversion to a smaller form in a TFEB-  
315 independent manner.

316

### 317 ***ROS function upstream of CD38 and of TFEB and TFE3***

318 CD38 is a fascinating transmembrane enzyme with complex membrane topol-  
319 ogy, subcellular localization, and regulation<sup>31</sup>. Upstream regulation of CD38 is  
320 poorly understood. It is thought that CD38 can be activated by reactive oxygen  
321 species (ROS) by an unknown mechanism<sup>33,34</sup>. Moreover, ROS activated  
322 TRPML1/MCOLN1 in HEK293 cells, presumably through CD38<sup>35</sup>. Therefore, we  
323 investigated the role of ROS in TFEB activation during infection.

324

325 First, we verified the accumulation of ROS and H<sub>2</sub>O<sub>2</sub> during infection with *S.*  
326 *aureus* in wild type macrophages (**Fig. 6A, B**). To our surprise, prior treatment  
327 with ROS-scavenging compounds N-acetyl cysteine (NAC) or N-acetyl cysteine  
328 aldehyde (NACA) completely prevented TFEB nuclear translocation by *S. aureus*  
329 (**Fig. 6C-G**) and *Salmonella* (**Fig. S6G-K**), suggesting that ROS were essential

330 for TFEB activation during infection. Conversely, treatment with CCCP, which  
331 uncouples the mitochondrial electron transport chain and elicits ROS, caused  
332 TFEB translocation in the absence of infection (**Fig. 6H, I, K**). Silencing of *Cd38*  
333 completely abrogated TFEB translocation caused by CCCP (**Fig. 6J, K**). Togeth-  
334 er, these data indicated that ROS, generated during infection with *S. aureus*, are  
335 necessary and sufficient for TFEB activation by infection, in a mechanism that  
336 requires CD38. However, the source of ROS during phagocytosis remained un-  
337 clear.

338

339 ***NADPH oxidase functions upstream of the ROS-CD38-TRPML1/MCOLN1-***  
340 ***CN-TFEB axis***

341 During phagocytosis, recruitment of NADPH oxidase (PHOX) to the maturing  
342 phagosome is a key event for phagolysosome maturation and bactericidal killing  
343 <sup>36</sup>. PHOX catalyzes the production of H<sub>2</sub>O<sub>2</sub> from NADPH oxidation, thus initiating  
344 the production of ROS in the phagolysosome <sup>37</sup>. Therefore, we examined PHOX  
345 as a potential source of ROS for CD38 activation during bacterial phagocytosis.

346

347 First, we examined the oxidative burst in macrophages harboring a deletion in  
348 *Nox2*, which encodes the gp91phox subunit. While wild type macrophages in-  
349 fected with *S. aureus* induced high levels of ROS and superoxide, *Nox2*<sup>-/-</sup> cells  
350 did not (**Fig. 7A, B**), consistent with PHOX being the main source of ROS in our  
351 infection assays. Consistent with the requirement for ROS to activate TFEB dur-



352 ing infection, *S. aureus* did not induce TFEB nuclear translocation in *Nox2*-  
353 deficient cells (**Fig. 7C-G**), suggesting that PHOX is required for TFEB activation  
354 by infection. In support of this conclusion, chemical inhibition of PHOX activity  
355 using apocynin completely prevented TFEB activation during *S. aureus* infection  
356 (**Fig. H-K**). We observed similar results with *Salmonella* (**Fig. S6L-P**). Together,  
357 these data suggested that PHOX functions upstream of TFEB, and that during  
358 bacterial infection its activity is essential for TFEB activation.

359

360 Immunofluorescence analysis revealed that *S. aureus* infection caused NOX2  
361 and CD38 colocalization to increase about 100% over baseline (**Fig. 7L-T**). We  
362 obtained similar results with *Salmonella* (**Fig. S6Q-T**). Taken together, this series  
363 of experiments supports a hypothetical model (**Fig. 7U**) in which phagocytosis of  
364 bacterial cells may cause activated PHOX and CD38 to localize to the same  
365 compartment, likely the phago-lysosome. ROS produced by PHOX may cause  
366 CD38 to produce NAADP, which could activate TRPML1/MCOLN1 and induce  
367  $Ca^{2+}$  export from the phago-lysosome/lysosome compartment.  $Ca^{2+}$  thus re-  
368 leased may activate calcineurin, which can dephosphorylate TFEB. Dephosphor-  
369 ylated TFEB can translocate into the nucleus, where it drives the expression of  
370 cytokines and chemokines, as previously demonstrated<sup>4,6</sup>. In addition, TFEB ac-  
371 tivation results in enhanced autophagy and lysosomal biogenesis, thus amplify-  
372 ing the phagocytic capacity of the cell via a positive feedback loop, and increases  
373 the degradative capacity of the cell via a positive feedforward loop<sup>7</sup>. However,  
374 this model did not account for the requirement of the PC-PLC/PrKD1 pathway for

375 TFEB activation.

376

377 ***Disruption of PC-PLC/PrKD1 signaling inhibits TRPML1/MCOLN1 locali-***  
378 ***zation to the lysosome***

379 A previous study showed that PrKD1 is required for TRPML1/MCOLN1  
380 transport from the Golgi apparatus to the lysosome in HeLa cells and human skin  
381 fibroblasts<sup>38</sup>. We tested if this is also a functional mechanism in macrophages.  
382 Using immunofluorescence in baseline murine macrophages, we observed low  
383 expression and localization to LAMP1-positive vesicles of TRPML1/MCOLN1  
384 (**Fig. S7A-C**). TRPML1/MCOLN1 expression was highly upregulated by treat-  
385 ment with ML-SA1 and by infection with *S. aureus* (**Fig. SD-I, T**). Such  
386 upregulation was expected, since *Mcoln1* is a direct TFEB target in macrophag-  
387 es, and is upregulated by TFEB activation<sup>6</sup>. Under *S. aureus* infection and ML-  
388 SA1 treatment, we also observed higher colocalization of TRPML1/MCOLN1 and  
389 LAMP1 (**Fig. S7D-F, J-L, S**). *S. aureus* infection caused a 100% increase in  
390 TRPML1/MCOLN1 – LAMP1 colocalization, which was partially abrogated by  
391 prior treatment with PrKD1 inhibitor kb-NB142-70 (**Fig. S7M-O, S**). kb-NB142-70  
392 also prevented the induced expression of TRPML1/MCOLN1 by *S. aureus* and  
393 MLSA1 (**Fig. S7T**). Together, these observations support the notion that PrKD1  
394 is necessary for TFEB activation because it is required for TRPML1/MCOLN1  
395 transport to the phagolysosome/lysosome compartment, where it is required for  
396 Ca<sup>2+</sup> export downstream of NAADP.

## 397 **Discussion**

398 In this article, we show a novel axis for TFEB activation in macrophages dur-  
399 ing phagocytosis of bacterial cells, which is essential for macrophage activation.  
400 Our observations support a model for a novel mechanism of pathogen sensing  
401 that is TLR-independent and is based on the phagocytic pathway. This pathway  
402 connects productive phagocytosis, presumably sensed by the recruitment of  
403 PHOX to the maturing phagosome. PHOX recruitment thus places the source of  
404 ROS in the same compartment as CD38, which may be endocytosed during  
405 phagocytosis of the bacterial particle. ROS generated by PHOX may activate  
406 CD38, as reported for lymphokine-activated killer cells and coronary arterial  
407 myocytes<sup>39,40</sup>, causing the accumulation of NAADP in the phagosome. After  
408 phago-lysosome fusion, TRPML1/MCOLN1 may come into contact with this res-  
409 ervoir of NAADP, thus triggering the release of lysosomal Ca<sup>2+</sup> into the cytosol. In  
410 the cytosol, Ca<sup>2+</sup> activates calcineurin, which dephosphorylates TFEB and ena-  
411 bles its nuclear import. In the nucleus, TFEB drives the expression of a large ma-  
412 jority of genes that are induced upon pathogen phagocytosis. Such gene induc-  
413 tion may require direct and indirect TFEB-dependent mechanisms. As far as we  
414 can tell, TFE3 is regulated in a similar manner.

415

416 Likewise, we found that bacterial molecules activate TFE3 and TFEB through  
417 a TLR-independent mechanism. These observations and the hypothetical model  
418 they support provide an explanation for previous, intriguing observations that

419 phagocytosis is sufficient to trigger TFEB nuclear translocation, but only if the  
420 phagocytic cup is able to close <sup>7</sup>. In this model, ROS serve dual functions as a  
421 bactericidal agent in the phago-lysosome, and as a signal to activate CD38 and  
422 initiate the signal cascade that results in TFEB/TFE3 activation. Since both  
423 PHOX- and mitochondria-derived ROS activated TFEB and TFE3, this provides  
424 redundant mechanisms of ROS production that report on phagocytosis and mito-  
425 chondrial integrity. Thus, the model predicts that any condition that leads to  
426 PHOX activation or mitochondrial disruption, increasing ROS, would result in  
427 TFEB/3 activation (at least, in macrophages). This has important implications for  
428 homeostasis and disease.

429

430 Since our discovery of the key role of TFEB in the transcriptional host re-  
431 sponse to infection in macrophages <sup>4</sup>, many studies have independently shown  
432 that TFEB and/or TFE3 greatly contribute to innate immunity against a large  
433 number of bacterial pathogens <sup>13,15,41</sup>. In addition, several signaling components  
434 have been identified in the regulation of TFEB/3, including AGS3 during LPS  
435 stimulation, the activation of TFEB by IFN- $\gamma$ , and the contribution of  
436 AMPK/mTORC1 regulation by several mechanisms <sup>42,43</sup>. Moreover, at least one  
437 example of bacterial modulation of TFEB has been elucidated, particularly how  
438 *Mycobacterium tuberculosis* represses TFEB through *mir-33* and *mir-33\** <sup>44</sup>. The-  
439 se discoveries underscore the central importance of TFEB/TFE3 as key contribu-  
440 tors to the host response to infection, and provide a strong rationale for complete  
441 understanding of the contributions of the novel PHOX/CD38/MCOLN1/TFEB

442 pathway described herein in distinct infectious diseases.

443

444 The events that occur downstream of TFEB/3 activation are of considerable in-  
445 terest. Prior studies demonstrated that TFEB and TFE3 have redundant and non-  
446 redundant functions important for the induction of key immune signaling mole-  
447 cules, such as intracellular signaling pathway components and extracellular cyto-  
448 kines and chemokines in LPS-stimulated macrophages <sup>6</sup>. Here we show that this  
449 is also true in the case of bacterial phagocytosis. Thus, TFEB/3 are predicted to  
450 be key contributors to the function of cellular networks in tissues that are under  
451 pathogenic attack, both in the induction of antimicrobial responses and in the re-  
452 cruitment of effector cells of the innate and adaptive immune systems.

453

454 Furthermore, we show that TFEB activation in macrophages induces  
455 lysosomal biogenesis, including the induction of TRPML1/MCOLN1 expression.  
456 Enhanced lysosomal biogenesis increases the availability of TRPML1/MCOLN1-  
457 containing lysosomes for fusion with PHOX/CD38-positive maturing  
458 phagosomes, thus enacting a positive phagocytosis feedback loop. In addition,  
459 prior studies showed how TFEB activation in macrophages leads to increased  
460 autophagy <sup>45-47</sup>, consistent with results in many other cell types. Thus, activation  
461 of the PHOX/CD38/TRPML1/CN/TFEB axis drives a positive phagocytosis  
462 feedforward loop that enhances the compartment that is poised to receive the  
463 mature phagolysosome for degradation, and enhances lysosomal exocytosis of  
464 remaining bacterial debris.

465

466        In summary, our studies reveal a heretofore unknown mechanism of macro-  
467 phage activation that is activated by phagocytosis of bacterial cells. Such mech-  
468 anism is parallel to better-understood TLR-mediated pathogen detection mecha-  
469 nisms. A key challenge for the future is to understand how diverse pathogen-  
470 detection pathways interact within an integrated regulatory network to produce a  
471 cellular response that is tailored to each particular pathogenic challenge. Addi-  
472 tionally, understanding how pathogens have evolved to circumvent this new axis  
473 may help understand microbial pathogenesis and reveal new mechanisms to  
474 safely manipulate it for therapeutic purposes.

## 475 **Materials and Methods**

### 476 ***Isolation and differentiation of Bone Marrow Derived macrophages***

#### 477 ***(BMDMs)***

478 Femurs and tibias from 8-12 weeks old mice were separated and cleaned.  
479 Bone marrow was flushed into 50 ml tubes under the sterile hood. Bone marrow  
480 was passed through the bone until the color of the bone turned white. After cen-  
481 trifugation at 1500 rpm for 5 minutes at 4 °C, cell pellets were resuspended and  
482 plated in BMDM media: DMEM (Fisher Scientific, MT10102CV), FBS 10%  
483 (Thermo Fisher, 16000069), AA 1% (Life Technologies, 15240-062), L-glutamine  
484 1% (Life Technologies, 25030-081), MEN NEA AA 1% (Life Technologies,  
485 11140-050), 2-Mercapto 0.1% (Life Technologies, 21985), IL-3 5 ng/ml  
486 (Peprotech: 213-13), MCSF 5 ng/ml (Peprotech: 315-02). Cell were used for ex-  
487 periments after 1 week of differentiation. To produce immortalized BMDMs, cells  
488 were transformed by CreJ2 virus<sup>48</sup>.

489

### 490 ***Cell culture, transfection and Imaging***

491 RAW264.7 and iBMDM cells were grown in Dulbecco's Modified Eagle's Me-  
492 dium (DMEM) - high glucose (Sigma-Aldrich, D6429-500ML) containing 10% en-  
493 dotoxin tested FBS (Thermo Fisher, 16000044), 1% Antibiotic-Antimycotic (Life  
494 Technologies 15240-062). Cells were passage 4 to 12 times. iBMDM GFP-TFEB  
495 stably transfected cells were created using pEGFP-N1-TFEB (pEGFP-N1-TFEB  
496 was a gift from Shawn Ferguson, Addgene plasmid # 38119), Lipofectamine

497 3000 (Thermo Fisher, L3000008) used according to manufacturer's instructions,  
498 and G418 sulfate (Life Technologies, 10131) used for selection. 10 days after se-  
499 lection, stable cells were separated by FACS. For Imaging we used 96-Well Op-  
500 tical-Bottom Plates (Thermo Fisher, 165305).  $6 \times 10^4$  cells were seeded in each  
501 well. At the end of the experiments, cells were fixed using 4% paraformaldehyde  
502 (Sigma-Aldrich, 158127) and incubated with Hoechst stain (Anaspec, AS-83218)  
503 at room temperature for 20 minutes as nuclear staining. For lysotracker staining,  
504 LysoTracker Red DND-99 (Thermo Fisher, L7528) was added to the media 30  
505 minutes before fixing according to the manufacture instruction. Image acquisition  
506 was automatically performed using a Cytation3 Imaging Plate Reader (Biotek).  
507 The N/C ratio was measured using CellProfiler (Broad Institute), as described in  
508 <sup>5</sup>. Colocalization analysis was performed using ImageJ software (NIH).

509

### 510 ***siRNA Knockdown***

511 siRNA compounds were purchased from Dharmacon RNAi Technologies.  
512 siGENOME NonTargeting siRNA #1 (D-001210-01-05). siGENOME Mouse Cd38  
513 (12494) siRNA - SMARTpool (M-058632-01- 0005). siGENOME Mouse Ppp3cb  
514 (19056) siRNA (M-063545-00-0005). siGENOME Mouse Ppp3r1 (19058) siRNA  
515 (M-040744-01-0005). siGENOME Mouse Mcoln1 (94178) siRNA (M-044469-00-  
516 0005). We used Lipofectamine RNAiMAX (Thermo Scientific, 13778030) for  
517 transfection according to manufacturer's instructions.

518



519 ***Bacterial strains***

520 *Salmonella enterica* serovar Typhimurium SL1344 wild type is a gift from Brian  
521 Coombes (McMaster University, Canada), *Staphylococcus aureus* NCTC8325 is  
522 a gift from Fred Ausubel, MGH Research Institute, USA.

523

524 ***In vitro infection***

525 Bacteria were grown overnight at 37 °C in LB medium (Difco, BD) with 100  
526 µg/ml streptomycin for *Salmonella* and Columbia medium (Difco, BD) with  
527 10 µg/ml Nalidixic acid for *S. aureus*. The following day cultures were diluted 1:50  
528 in the same medium and grown at 37 °C for 3 h to late-exponential phase,  
529 washed twice in cold PBS, and cells were infected with MOI 10 for *S. aureus* and  
530 MOI 10 for *S. enterica*, as in (Engelenburg and Palmer, 2010; Najibi et al., 2016;  
531 Trieu et al., 2009; Visvikis et al., 2014). For gentamycin antibiotic (AB) - killed  
532 bacteria, before addition to cells, gentamicin (100 µg/ml) was added to washed  
533 bacteria in PBS for 2 hours and 100% killing of the bacteria was confirmed by  
534 culture for 48 h on LB-streptomycin agar at 37°C. The appropriate amounts of  
535 bacteria were resuspended in DMEM 10 % FBS without antibiotic.

536

537 ***Immunofluorescence***

538 After treatment, cells were fixed with 4% paraformaldehyde (PFA) pH 7.4 at  
539 room temperature for 10 min and washed 3 times in PBS (Gibco Life Technolo-  
540 gies,10010) for 5 min each. PFA was neutralized with 50 mM NH<sub>4</sub>Cl in PBS at

541 room temperature for 10 minutes with agitation. After 3 washes with PBS, cells  
542 were permeabilized with 0.1% Triton X in PBS at room temperature on agitator  
543 for 5 min and then blocked with 5% bovine serum albumin (Sigma-Aldrich,  
544 A9647) in PBS for 1 h. After 3 washes with PBS cells were incubated with prima-  
545 ry antibodies for 2 hours. Anti-TFEB Antibody (Cell Signaling, 4240). Anti-TFE3  
546 antibody (Sigma-Aldrich, HPA023881-100UL). Anti-CD38 antibody (Abcam,  
547 ab24978). Anti-NOX2/gp91phox antibody (Abcam, ab80508). Anti-LAMP1 (Cell  
548 Signaling Technology, 9091). Anti-Mucolipin 1 (MCOLN1) (C-Term) antibody  
549 (Antibodies-Online, ABIN571446). Cells were washed thrice in PBS and incubat-  
550 ed with the fluorescent secondary antibody plus Hoechst stain (Anaspec, AS-  
551 83218) at room temperature for 1 h. Image acquisition was performed using a  
552 Cytation3 imaging plate reader (Biotek).

553

#### 554 ***Immunoblotting***

555 Cells were washed 3 times with PBS, harvested, and lysed with 1X SDS sam-  
556 ple buffer Blue Loading Pack (Cell Signaling, 7722) at 100  $\mu$ l per well of 6-well  
557 plate. Lysates were heated at 100 °C for 5 min and then centrifuged for 5 min.  
558 The supernatant was collected and sonicated, gel electrophoresis was performed  
559 using Novex 4-20% Tris-Glycine Mini Gels (Invitrogen, XP04200BOX), and were  
560 then transferred onto nitrocellulose (Life Technologies, LC2009). After wash with  
561 TBS (Life Technologies, 28358) for 5 minutes, membranes were soaked in block-  
562 ing buffer containing 1X TBS with 5% BSA for 1 hour at room temperature. After  
563 3 washes with TBS-Tween (Life Technologies, 28360), membranes were incu-

564 bated overnight at 4 °C with primary antibodies and gentle agitation. Next mem-  
565 branes were washed thrice with TBS-Tween and incubated with HRP-conjugated  
566 secondary antibody (Cell Signaling, 7074 1:2000) for 1 h at room temperature  
567 with gentle agitation. Membranes were then washed with TBS-Tween and incu-  
568 bated with LumiGLO® (Cell signaling, 7003) for 1 min and exposed to x-ray film  
569 (Denville Scientific, E3012). Primary antibodies and dilutions that were used are  
570 as follows:  $\beta$ -actin antibody (Cell Signaling Technology, 4967, 1:1000), Anti-  
571 CD38 Antibody (Cell Signaling Technology, 14637S 1:1000), Anti-TLR4 antibody  
572 (). Anti-TLR2 antibody (). Anti-Mucolin 1 (MCOLN1) (C-Term) antibody (Anti-  
573 bodies-Online, ABIN571446 1:1000).

574

### 575 ***Drugs and reagents***

576 Lipopolysaccharides (LPS) from *S. enterica* serotype Typhimurium (Sigma-  
577 Aldrich, L6143-1MG, 10ug/ml): Peptidoglycan (PGN) from *S. aureus* (Invivogen,  
578 tlrl-pgns2): Monophosphoryl Lipid A (MPLA-SM) (Invivogen, tlrl-mpla): ML-SA1  
579 (Sigma Aldrich, SML0627) Ionomycin (Cayman Chemical Company, 10004974):  
580 FK-506 (Cayman Chemical Company, 10007965): BAPTA AM (Cayman Chemi-  
581 cal Company, 15551): Ned-19 (Cayman Chemical Company, 17527): Kuromanin  
582 (Cayman Chemical Company, 16406): Apigenin (Cayman Chemical Company,  
583 10010275): CCCP (Cayman Chemical Company, 25458): N-acetyl-L-Cysteine  
584 (NAC) (Cayman Chemical Company, 20261): N-acetyl-L-Cysteine amide (NACA)  
585 (Cayman Chemical Company, 25866): Apocynin (Cayman Chemical Company,  
586 11976): D609 (Cayman Chemical, 13307, 50  $\mu$ M): kb NB 142-70 (Cayman

587 Chemical Company, 18002).

588

### 589 ***ROS/Superoxide Detection Assay***

590 Cellular ROS/Superoxide Detection Assay Kit (Abcam, ab139476) was used  
591 according to the manufacture instruction. Mean fluorescence intensity was calcu-  
592 lated by Biotek Gen5 Data Analysis Software.

593

### 594 ***RNA Sequencing and Differential Expression Analysis***

595 RAW264.7 dKO were a one-time gift from Rosa Puertollano (NHLBI). Infection  
596 was performed as described in *In Vitro Infection*, in three independent replicates.  
597 RNA was extracted by TRIzol Plus RNA Purification Kit (Thermo Fisher,  
598 12183555). Whole cell RNA was submitted to BGI Inc for ribosomal RNA deple-  
599 tion, library construction, and sequencing on Illumina NextSeq machines. Reads  
600 were trimmed and quality-filtered by BGI. Clean reads were mapped to the  
601 GRCm38 mouse reference transcriptome using Salmon v0.13.1 and transcript-  
602 quantified (Patro et al., 2017). Salmon quant outputs were analyzed using  
603 tximport and DESeq2 v1.22.2 in R (Love et al., 2014). DESeq2 output counts  
604 were used as input for interactive analysis and data plotting using DEBrowser  
605 1.10.9 in R (Kucukural et al., 2019). Differentially expressed (fold change  $\geq 2$ ;  
606  $P_{adj} \leq 0.01$ ; filter genes with fewer than 10 counts) gene sets were used as input  
607 for g:Profiler v0.6.6 online tools (Raudvere et al., 2019).

608

609 ***ELISA Assay***

610 Concentrations of IL-1 $\alpha$ , IL-1 $\beta$ , IL-6 and TNF- $\alpha$  were measured by en-  
611 zyme-linked immunosorbent assays (ELISAs) using kits purchased from R&D  
612 Systems (DY400-05, DY401-05, DY406-05, DY8234-05, DY410-05, respective-  
613 ly). All incubation periods occurred at room temperature, and plates were washed  
614 with Tris buffered saline (TBS) containing 0.05% Tween 20 (Bethyl Laboratories,  
615 E106) after each step. Briefly, clear microplates (R&D Systems, DY990) were  
616 incubated overnight with capture antibody. Plates were blocked for one hour us-  
617 ing TBS containing 1% BSA (Bethyl Laboratories, E104). Samples were added  
618 undiluted (IL-1 $\alpha$ , IL-1 $\beta$ , IL-6) or diluted 1:10 in TBS containing 1% BSA (TNF- $\alpha$ )  
619 and plates were incubated for two hours. Detection antibody was added, and  
620 plates were incubated for two hours. Streptavidin-Horseradish Peroxidase (Strep-  
621 HRP) was added, and plates were incubated for 20 minutes. TMB One Compo-  
622 nent HRP Microwell Substrate (Bethyl Laboratories, E102) was added, and reac-  
623 tion was stopped after 20 minutes using ELISA Stop Solution (Bethyl Laborato-  
624 ries, E115). Optical densities were measured at 450 nm and 540 nm using  
625 SpectraMax Plus 384 Microplate Reader with SoftMax Pro software. Measure-  
626 ments at 540 nm were subtracted from measurements at 450 nm to correct for  
627 optical impurities of the plates, per manufacturer's recommendations. Concentra-  
628 tions of samples were interpolated from each standard curve using Prism 8. Data  
629 are represented as mean  $\pm$  SEM.

630

631 ***LDH Assay***

632 Lactate Dehydrogenase (LDH) activity was measured using an LDH assay kit  
633 purchased from Abcam (ab102526). LDH assay was performed following manu-  
634 facturer's guidelines. Briefly, samples were added to a clear microplate (R&D  
635 Systems, DY990). Reaction mix was made using supplied LDH Assay Buffer and  
636 LDH Substrate Mix. Reaction mix was then added to each sample. Optical densi-  
637 ties were measured at 450 nm using SpectraMax Plus 384 Microplate Reader  
638 with SoftMax Pro software. The amount of NADH in each sample was interpolat-  
639 ed from the standard curve using Prism 8. LDH activity was quantified by dividing  
640 the amount of NADH in each sample by the product of the reaction time in  
641 minutes and the original volume of sample added into the reaction well in mL.  
642 LDH activity was reported in mU/mL and plotted as mean  $\pm$  SEM.

## 643 **Figure Legends**

644 **Figure 1. Gram+ bacterial cells and ligands activate TFE3. A-H.** GFP-  
645 TFEB immortalized BMDM (iBMDMs) were infected with *S. aureus* (MOI = 10) for  
646 3 h. Incubation with 10 µg/ml PGN from *S. aureus* was 3 h. Cells were fixed and  
647 processed for anti-TFE3 immunofluorescence staining. Shown are representative  
648 images, and quantification of three biological replicates (n = 450). **A.** DMSO con-  
649 trol, **B.** *S. aureus* infection, and **C.** *S. aureus* PGN (10 µg/ml). **D.** DMSO control,  
650 **E.** *S. aureus* infection, **F.** *S. aureus* PGN. **G.** GFP-TFEB intensity in the nucleus  
651 compared to the cytoplasm (N/C ratio) measured using CellProfiler. \*\*\*\* p ≤  
652 0.0001 (one-way ANOVA followed by Tukey's post-hoc test). **(H)** Anti-TFE3 fluo-  
653 rescence N/C ratio measured using CellProfiler. \*\*\*\* p ≤ 0.0001 (one-way  
654 ANOVA followed by Tukey's post-hoc test). **I-N.** GFP-TFEB iBMDMs were infect-  
655 ed with *S. aureus* or incubated with *S. aureus* PGN as above, and stained with  
656 LysoTracker. Shown are representative images and quantification of three biolog-  
657 ical replicates (n = 60). **I.** DMSO control. **J.** *S. aureus* infection, and **K.** *S. aureus*  
658 PGN. **L-N.** Higher magnification micrographs for DMSO control (**L**), *S. aureus*  
659 (**M**), and PGN (**N**). **O.** LysoTracker intensity per cell (MFI/cell) measured with  
660 CellProfiler. \*\*\*\* p ≤ 0.0001 (one-way ANOVA followed by Tukey's post-hoc test).  
661 **P-R.** Comparison of LysoTracker intensities in cells with TFEB cytoplasmic locali-  
662 zation (C) with that in cells with nuclear localization (N) following incubation with  
663 DMSO (**P**), *S. aureus* (**Q**), or PGN (**R**). \*\*\*\* p ≤ 0.0001 (two-sample two-tailed  
664 unpaired *t* test).

665

666 **Figure 2. TFEB and TFE3 are required for the macrophage transcriptional**  
667 **response to *S. aureus*. A-E.** Wild type (WT) and *Tfeb Tfe3* double knockout  
668 (dKO) RAW264.7 cells were infected as described in *Methods* for 3 h. N = 3 bio-  
669 logical replicates. **A.** Heat map showing expression of genes that were differen-  
670 tially expressed in wild type cells. Shown are baseline and infected conditions, in  
671 both cell lines. Two groups of genes with defective induction in dKO cells are in-  
672 dicated with black boxes. **B.** Heat map showing expression of M1 and M2 marker  
673 genes. Colors indicate direction and magnitude of expression per row; circle di-  
674 ameter is proportional to absolute expression. Grey indicates no expression de-  
675 tected. **C.** Volcano plot showing differential gene expression in infected dKO cells  
676 relative to infected WT cells. Blue color denotes downregulation in dKO cells; red  
677 indicates upregulation in dKO cells. Green highlights noteworthy innate immunity  
678 genes, with corresponding adjacent labels. **D.** Pie chart showing percent of  
679 genes that are upregulated in infected v uninfected WT cells, and which are  
680 TFEB/3-dependent. **E.** Reactome pathway over-representation analysis of  
681 TFEB/3-dependent genes, plotting adjusted P values for each category (P<sub>adj</sub>). **F.**  
682 Verification of TFEB expression in *Tfeb*<sup>flox/flox</sup> (WT) and *Tfeb*<sup>ΔLysM</sup> (*Tfeb*<sup>-/-</sup>) iBMDMs  
683 by anti-TFEB immunoblot. **G-K.** Wild type (WT) and *Tfeb*<sup>ΔLysM</sup> (*Tfeb*<sup>-/-</sup>) iBMDMs  
684 were incubated with PBS (Ctrl) or infected with *S. aureus* (Sa, MOI = 10). Con-  
685 centrations of IL-1α (**G**), IL-1β (**H**), IL-6 (**I**), TNF-α (**J**), and lactate dehydrogenase  
686 activity (LDH, cytolysis control, **K**) were measured in culture supernatants 13 h  
687 following infection, by ELISA and LDH assay, respectively. N = 5-6, \*p < 0.05, \*\*p



688 < 0.01, \*\*\*p < 0.001, \*\*\*\*p < 0.0001, one-way ANOVA followed by Tukey's post-  
689 hoc test.

690

691 **Figure 3. TLR signaling is dispensable for TFEB activation. A-N.** Primary  
692 BMDMs from WT and *Myd88 Trif* double knockout mice (*Myd88 Trif* dKO) were  
693 infected, fixed, and processed for anti-TFEB immunofluorescence staining. TFEB  
694 fluorescence N/C ratio per cell was measured using CellProfiler (n = 250). Shown  
695 are representative images and quantification of three biological replicates. **A, B.**  
696 DMSO control (t = 6 h); **C, D.** *Salmonella* Typhimurium (St; MOI = 1, t = 6 h). **E,**  
697 **F.** Monophosphoryl lipid A (MPLA, 1 µg/ml, t = 6 h). **G, H.** *Salmonella*  
698 Typhimurium lipopolysaccharide (LPS, 1 µg/ml, t = 6 h). **I, J.** *S. aureus* (Sa, MOI  
699 = 10, t = 3 h). **K, L.** *S. aureus* peptidoglycan (PGN, 10 µg/ml, t = 3 h). **M, N.**  
700 Quantification of TFEB N/C ratio per cell in WT (**M**) and *Myd88 Trif* dKO (**N**) cells.  
701 \*\*\* p ≤ 0.001 (one-way ANOVA followed by Tukey's post-hoc test).

702

703 **Figure 4. TFEB activation is mediated by TRPML1/MCOLN1, Ca<sup>2+</sup>, and**  
704 **calcineurin. A-E.** GFP-TFEB iBMDMs were treated with DMSO without infection  
705 (t = 3 h, **A**) or treated for 3 h and subsequently infected with *S. aureus* (**B**, MOI =  
706 10, t = 3 h). In parallel, cells were treated with BAPTA (**C**, 10 µM, t = 3 h) or  
707 FK506 (**D**, 5 µM, t = 6 h) and subsequently infected with *S. aureus* (MOI = 10, t =  
708 3 h). **E.** Quantification of GFP-TFEB N/C Ratio by CellProfiler (3 biological repli-  
709 cates, n = 350 cells). \*\*\*\* p ≤ 0.0001 (one-way ANOVA followed by Tukey's post-  
710 hoc test). **F-K.** GFP-TFEB iBMDMs were treated with scrambled (Scr, **F**) or

711 siRNA against *Ppp3cb* (**G**), *Ppp3r1* (**H**) for 48 h. Cells were treated with Scr (**I**),  
712 *Ppp3cb* (**J**), or *Ppp3r1* (**K**) siRNA for 48 h prior to infection with *S. aureus* (MOI =  
713 10, t = 3 h). **L**. GFP-TFEB N/C Ratio by CellProfiler (3 biological replicates, n =  
714 210 cells). \*\*\*  $p \leq 0.001$  (one-way ANOVA followed by Tukey's post-hoc test). **M**,  
715 **N**. GFP-TFEB iBMDMs were treated with DMSO (**M**, t = 6 h) or Ionomycin (**N**, 10  
716  $\mu\text{M}$ , t = 6 h). **O**. GFP-TFEB N/C Ratio by CellProfiler (3 biological replicates, n =  
717 350 cells). \*\*\*\*  $p \leq 0.0001$  (one-way ANOVA followed by Tukey's post-hoc test).  
718 **P-S**. GFP-TFEB iBMDMs were treated with scrambled (Scr, **P**) or siRNA against  
719 *Mcoln1* (**Q**) for 48 h. Cells were treated with Scr (**R**) or *Mcoln1* (**S**) siRNA for 48 h  
720 prior to infection with *S. aureus* (MOI = 10, t = 3 h). **T**. GFP-TFEB N/C Ratio by  
721 CellProfiler (3 biological replicates, n = 300 cells). \*\*\*  $p \leq 0.001$  (one-way ANOVA  
722 followed by Tukey's post-hoc test). **U**, **V**. GFP-TFEB iBMDMs were treated with  
723 DMSO (**U**, t = 3 h) or ML-SA1 (**V**, 10  $\mu\text{M}$ , t = 3 h). **W**. GFP-TFEB N/C Ratio by  
724 CellProfiler (3 biological replicates, n = 355 cells). \*\*\*\*  $p \leq 0.0001$  (two-sample  
725 two-sided *t* test).

726

727 **Figure 5. CD38 activates TFEB through NAADP and TRPML1/MCOLN1. A-**  
728 **E**. GFP-TFEB iBMDMs were treated with DMSO without infection (DM., t = 6 h,  
729 **A**) or treated for 6 h and subsequently infected with *S. aureus* (**B**, MOI = 10, t = 3  
730 h). In parallel, cells were treated with Ned-19 (**C**, Ned., 10  $\mu\text{M}$ , t = 4 h),  
731 Kuromanin (**D**, Kuro., 100  $\mu\text{M}$ , t = 6 h), or Apigenin (**E**, Api., 100  $\mu\text{M}$ , t = 6 h) and  
732 subsequently infected with *S. aureus* (MOI = 10, t = 3 h). **F**. Quantification of  
733 GFP-TFEB N/C Ratio by CellProfiler (3 biological replicates, n = 200 cells). \*\*\*\*  $p$

734  $\leq 0.0001$  (one-way ANOVA followed by Tukey's post-hoc test). **G-I.** GFP-TFEB  
735 iBMDMs were treated with scrambled (Scr, **G**) or siRNA for 48 h. Cells were  
736 treated with Scr (**H**) or *Cd38* (**I**) siRNA for 48 h prior to infection with *S. aureus*  
737 (MOI = 10, t = 3 h). **J.** GFP-TFEB N/C Ratio by CellProfiler (3 biological repli-  
738 cates, n = 350 cells). \*\*\*  $p \leq 0.001$  (one-way ANOVA followed by Tukey's post-  
739 hoc test). **K-M.** GFP-TFEB iBMDMs were treated with DMSO (DM., t = 2 h, **K**) or  
740 treated with scrambled siRNA (Scr, t = 48 h) and subsequently incubated with  
741 NAADP-AM (100 nM, t = 2 h, **L**). In parallel, cells were treated with *Mcoln1*  
742 siRNA (t = 48 h) and subsequently incubated with NAADP-AM (100 nM, t = 2 h,  
743 **M**). **N.** Quantification of GFP-TFEB N/C Ratio by CellProfiler (3 biological repli-  
744 cates, n = 300 cells). \*\*\*\*  $p \leq 0.0001$  (one-way ANOVA followed by Tukey's post-  
745 hoc test). **O, P.** CD38 immunofluorescence in wild type primary BMDM. PBS con-  
746 trol (**O**) and *S. aureus* infection (MOI = 10, t = 2 h, **P**). **Q.** CD38 immunoblot of  
747 whole cell lysates from wild type and *Tfeb* <sup>$\Delta$ LysM</sup> (*Tfeb*<sup>-/-</sup>) iBMDMs incubated with  
748 PBS or infected with *S. aureus* (MOI = 10, t = 3 h).  $\beta$ -actin is loading control.  
749 Representative of three biological replicates.

750

751 **Figure 6. ROS activate TFEB through CD38.** ROS (**A**) and superoxide (**B**)  
752 generated in wild type primary BMDM during infection with *S. aureus* (MOI = 10, t  
753 = 1 h) shown as mean fluorescence intensity (MFI) per cell and measured with  
754 Gen5 (n = 50 cells, 3 biological replicates). \*\*\*\*  $p \leq 0.0001$  (two-sided two-sample  
755 *t* test). **C-F.** GFP-TFEB iBMDMs were treated with DMSO without infection (DM.,  
756 t = 4 h, **C**) or treated for 4 h and subsequently infected with *S. aureus* (**D**, MOI =

757 10, t = 3 h). In parallel, cells were treated with NAC (**E**, 5 mM, t = 4 h) or NACA  
758 (**F**, 1 mM, t = 4 h) and subsequently infected with *S. aureus* (MOI = 10, t = 3 h).  
759 **G**. Quantification of GFP-TFEB N/C Ratio by CellProfiler (3 biological replicates,  
760 n = 250 cells). \*\*\* p ≤ 0.001, \*\*\*\* p ≤ 0.0001 (one-way ANOVA followed by  
761 Tukey's post-hoc test). **H-J**. GFP-TFEB iBMDMs were treated with DMSO (DM., t  
762 = 3 h, **H**) or treated with scrambled siRNA (Scr, t = 48 h) and subsequently incu-  
763 bated with CCCP (10 μM, t = 3 h, **I**). In parallel, cells were treated with *Cd38*  
764 siRNA (t = 48 h) and subsequently incubated with CCCP (10 μM, t = 3 h, **J**). **K**.  
765 Quantification of GFP-TFEB N/C Ratio by CellProfiler (3 biological replicates, n =  
766 355 cells). \*\*\*\* p ≤ 0.0001 (one-way ANOVA followed by Tukey's post-hoc test).  
767

768 **Figure 7. Infection induced ROS and TFEB activation require NADPH ox-**  
769 **idase.** ROS (**A**) and superoxide (**B**) generated in wild type and *Nox2<sup>-/-</sup>* primary  
770 BMDM during infection with *S. aureus* (MOI = 10, t = 1 h) shown as mean fluo-  
771 rescence intensity (MFI) per cell and measured with Gen5 (n = 200 cells, 3 bio-  
772 logical replicates). \*\*\*\* p ≤ 0.0001 (two-sided two-sample *t* test). **C-F**. TFEB im-  
773 munofluorescence in wild type and *Nox2<sup>-/-</sup>* primary BMDM. PBS controls (**C**, **E**)  
774 and infected cells (MOI = 10, t = 3 h, **D**, **F**). **G**. Quantification of TFEB N/C Ratio  
775 by CellProfiler (3 biological replicates, n = 200 cells). \*\*\* p ≤ 0.001, ns: p =  
776 0.4399 (one-way ANOVA followed by Tukey's post-hoc test). **H-J**. GFP-TFEB  
777 iBMDMs were treated with DMSO without infection (DM., t = 4 h, **H**) or treated for  
778 4 h and subsequently infected with *S. aureus* (**I**, MOI = 10, t = 3 h). In parallel,  
779 cells were treated with Apocynin (**J**, 10 μM, t = 4 h) and subsequently infected

780 with *S. aureus* (MOI = 10, t = 3 h). **K.** Quantification of GFP-TFEB N/C Ratio by  
781 CellProfiler (3 biological replicates, n = 250 cells). \*\*\*  $p \leq 0.001$  (one-way ANOVA  
782 followed by Tukey's post-hoc test). **L-S.** Immunofluorescence detection of NOX2  
783 and CD38 in wild type primary BMDM. Cells were incubated with PBS (**L-O**) or  
784 infected with *S. aureus* (MOI = 10, t = 3 h, **P-S**). **T.** Colocalization analysis of  
785 NOX2 and CD38. \*\*\*\*  $p \leq 0.0001$  (two-sided two-sample unpaired *t* test). **U.** Pro-  
786 posed hypothetical model for the phagocytosis-triggered activation of TFEB.

## 787 **Acknowledgments**

788 The authors are grateful to members of the Irazoqui laboratory, the Fitzgerald  
789 laboratory, the Program in Innate Immunity, and the Department of Microbiology  
790 and Physiological Systems for helpful insights and discussions. The Fitzgerald  
791 laboratory provided several knockout primary and immortalized BMDMs, and the  
792 Sasseti laboratory provided *Nox2* mutant mice and CreJ2 virus. This work was  
793 partially funded by grant R01GM101056 (JEI) from the National Institutes of  
794 Health. The content is solely the responsibility of the authors and does not nec-  
795 essarily represent the official views of the National Institutes of Health.

796

## 797 **Competing Interests**

798 The authors declare no competing interests.

799

## 800 **Author Contributions**

801 Conceptualization, JEI and MN; Methodology, JEI and MN; Investigation, MN,  
802 JAM, JEI, and HHH; Animals, JAM; Writing—original draft, JEI; Writing—review  
803 and editing, JEI, MN, JAM, and HH; Visualization, MN and JEI; Supervision, JEI;  
804 Funding acquisition, JEI.

## 805 **References**

806

807 1. Aderem, A. & Underhill, D. M. MECHANISMS OF PHAGOCYTOSIS IN  
808 MACROPHAGES. *Annu Rev Immunol* **17**, 593–623 (1999).

809

810 2. Lawrence, T. & Natoli, G. Transcriptional regulation of macrophage polariza-  
811 tion: enabling diversity with identity. *Nat Rev Immunol* **11**, 750 (2011).

812

813 3. Medzhitov, R. & Horng, T. Transcriptional control of the inflammatory re-  
814 sponse. *Nat Rev Immunol* **9**, 692–703 (2009).

815

816 4. Visvikis, O. *et al.* Innate Host Defense Requires TFEB-Mediated Transcription  
817 of Cytoprotective and Antimicrobial Genes. *Immunity* **40**, 896–909 (2014).

818

819 5. Najibi, M., Labed, S., Visvikis, O. & Irazoqui, J. An Evolutionarily Conserved  
820 PLC-PKD-TFEB Pathway for Host Defense. *Cell Reports* **15**, 1728–1742 (2016).

821

822 6. Pastore, N. *et al.* TFEB and TFE3 cooperate in the regulation of the innate  
823 immune response in activated macrophages. *Autophagy* **12**, 1–19 (2016).

824

825 7. Gray, M. A. *et al.* Phagocytosis Enhances Lysosomal and Bactericidal Proper-  
826 ties by Activating the Transcription Factor TFEB. *Curr Biology Cb* **26**, 1955–64  
827 (2016).

828

829 8. Puertollano, R., Ferguson, S. M., Brugarolas, J. & Ballabio, A. The complex  
830 relationship between TFEB transcription factor phosphorylation and subcellular  
831 localization. *Embo J* **37**, e98804 (2018).

832

833 9. Malavasi, F. *et al.* Evolution and function of the ADP ribosyl cyclase/CD38  
834 gene family in physiology and pathology. *Physiol Rev* **88**, 841–886 (2008).

835

836 10. Roberts, R. A. *et al.* Nitrate and Oxidative Stress in Toxicology and Dis-  
837 ease. *Toxicol Sci* **112**, 4–16 (2009).

838

839 11. Lin, M. T. & Beal, F. M. Mitochondrial dysfunction and oxidative stress in neu-  
840 rodegenerative diseases. *Nature* **443**, nature05292 (2006).

841

842 12. Halliwell, B. & Cross, C. Oxygen-derived species: their relation to human dis-  
843 ease and environmental stress. *Environ Health Persp* **102**, 5–12 (1994).

844

845 13. Raben, N. & Puertollano, R. TFEB and TFE3: Linking Lysosomes to Cellular  
846 Adaptation to Stress. *Annu Rev Cell Dev Bi* **32**, 1–24 (2015).

847

848 14. Martina, J. A. & Puertollano, R. Protein phosphatase 2A stimulates activation  
849 of TFEB and TFE3 transcription factors in response to oxidative stress. *J Biol*  
850 *Chem* **293**, 12525–12534 (2018).



851

852 15. El-Houjeiri, L. *et al.* The Transcription Factors TFEB and TFE3 Link the  
853 FLCN-AMPK Signaling Axis to Innate Immune Response and Pathogen Re-  
854 sistance. *Cell Reports* **26**, 3613-3628.e6 (2019).

855

856 16. Eswarappa, S., Negi, V., Chakraborty, S., Sagar, C. B. & Chakravortty, D.  
857 Division of the Salmonella-containing vacuole and depletion of acidic lysosomes  
858 in Salmonella-infected host cells are novel strategies of *Salmonella enterica* to  
859 avoid lysosomes. *Infect Immun* **78**, 68 79 (2010).

860

861 17. McGourty, K. *et al.* *Salmonella* Inhibits Retrograde Trafficking of Mannose-6-  
862 Phosphate Receptors and Lysosome Function. *Science* **338**, 963–967 (2012).

863

864 18. Fabregat, A. *et al.* The Reactome Pathway Knowledgebase. *Nucleic Acids*  
865 *Res gkx1132-* (2017). doi:10.1093/nar/gkx1132

866

867 19. Takeda, K. & Akira, S. TLR signaling pathways. *Semin Immunol* **16**, 3–9  
868 (2004).

869

870 20. Yamamoto, M. *et al.* Role of Adaptor TRIF in the MyD88-Independent Toll-  
871 Like Receptor Signaling Pathway. *Science* **301**, 640–643 (2003).

872

873 21. Medina, D. L. *et al.* Lysosomal calcium signalling regulates autophagy

- 874 through calcineurin and TFEB. *Nat Cell Biol* **17**, 288–299 (2015).
- 875
- 876 22. Paola, S., Scotto-Rosato, A. & Medina, D. TRPML1: The Ca(2+)retaker of the  
877 lysosome. *Cell Calcium* **69**, (2018).
- 878
- 879 23. Shen, D. *et al.* Lipid storage disorders block lysosomal trafficking by inhibiting  
880 a TRP channel and lysosomal calcium release. *Nat Commun* **3**, 731 (2012).
- 881
- 882 24. Zhang, F. & Li, P.-L. Reconstitution and Characterization of a Nicotinic Acid  
883 Adenine Dinucleotide Phosphate (NAADP)-sensitive Ca<sup>2+</sup> Release Channel  
884 from Liver Lysosomes of Rats. *J Biol Chem* **282**, 25259–25269 (2007).
- 885
- 886 25. Zhang, F., Jin, S., Yi, F. & Li, P. TRPML1 functions as a lysosomal  
887 NAADP-sensitive Ca<sup>2+</sup> release channel in coronary arterial myocytes. *J Cell*  
888 *Mol Med* **13**, 3174–3185 (2009).
- 889
- 890 26. Naylor, E. *et al.* Identification of a chemical probe for NAADP by virtual  
891 screening. *Nat Chem Biol* **5**, 220–226 (2009).
- 892
- 893 27. Kellenberger, E., Kuhn, I., Schuber, F. & Muller-Steffner, H. Flavonoids as  
894 inhibitors of human CD38. *Bioorg Med Chem Lett* **21**, 3939–3942 (2011).
- 895
- 896 28. Escande, C. *et al.* Flavonoid Apigenin Is an Inhibitor of the NAD<sup>+</sup>ase CD38

897 Implications for Cellular NAD<sup>+</sup> Metabolism, Protein Acetylation, and Treatment of  
898 Metabolic Syndrome. *Diabetes* **62**, 1084–1093 (2013).

899

900 29. Parkesh, R. *et al.* Cell-permeant NAADP: A novel chemical tool enabling the  
901 study of Ca<sup>2+</sup> signalling in intact cells. *Cell Calcium* **43**, 531–538 (2008).

902

903 30. Funaro, A. *et al.* CD38 functions are regulated through an internalization  
904 step. *J Immunol Baltim Md 1950* **160**, 2238–47 (1998).

905

906 31. ZOCCHI, E. *et al.* Ligand-induced internalization of CD38 results in intracellu-  
907 lar Ca<sup>2+</sup> mobilization: role of NAD<sup>+</sup> transport across cell membranes. *Faseb J*  
908 **13**, 273–283 (1999).

909

910 32. Kang, J. *et al.* The Role of CD38 in Fcγ Receptor (FcγR)-mediated Phagocy-  
911 tosis in Murine Macrophages. *J Biol Chem* **287**, 14502–14514 (2012).

912

913 33. Wilson, H. L. *et al.* ADP-ribosyl Cyclase and Cyclic ADP-ribose Hydrolase Act  
914 as a Redox Sensor A PRIMARY ROLE FOR CYCLIC ADP-RIBOSE IN  
915 HYPOXIC PULMONARY VASOCONSTRICTION. *J Biol Chem* **276**, 11180–  
916 11188 (2001).

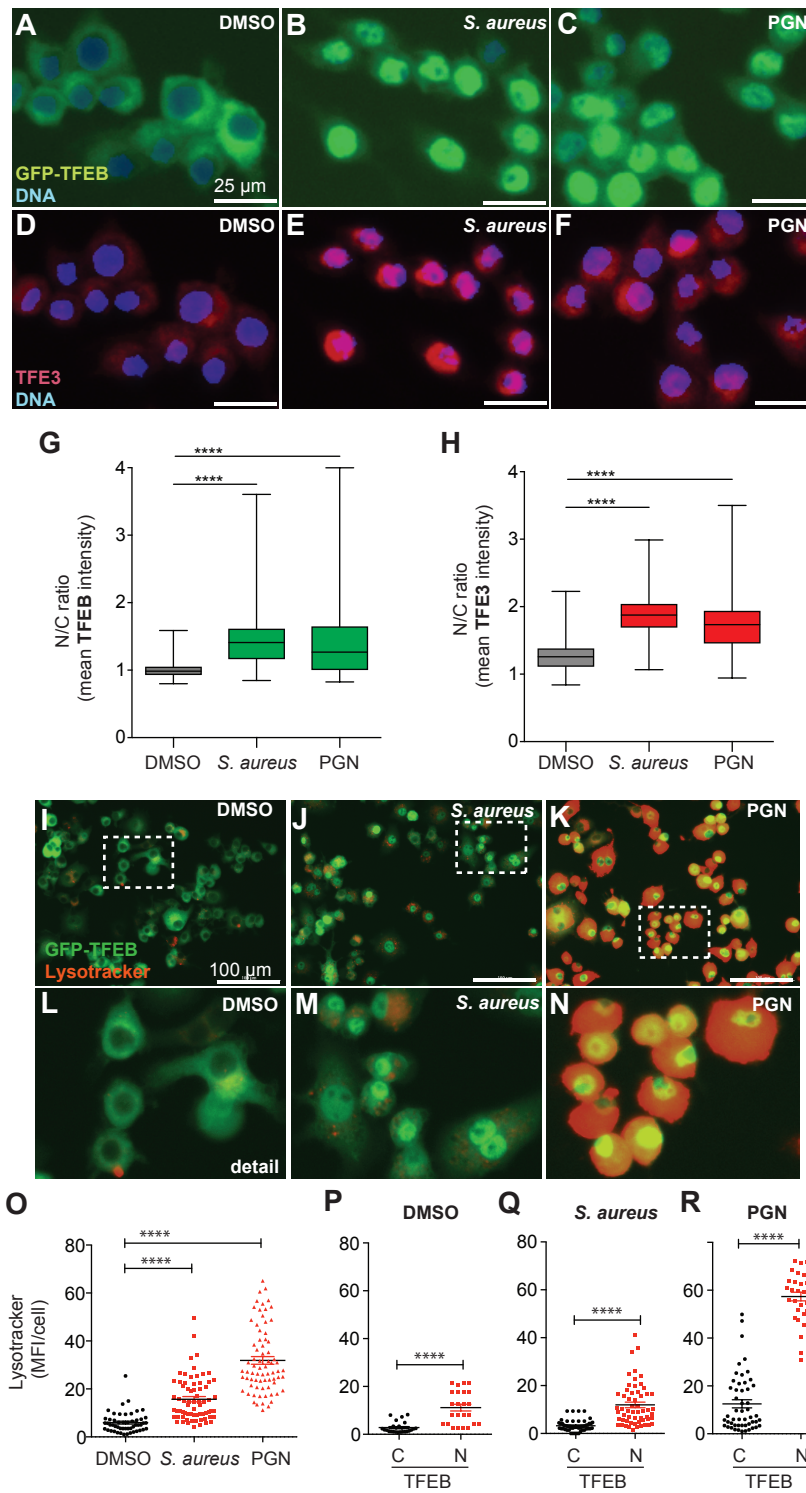
917

918 34. Zhang, A. Y., Yi, F., Teggatz, E. G., Zou, A.-P. & Li, P.-L. Enhanced produc-  
919 tion and action of cyclic ADP–ribose during oxidative stress in small bovine coro-

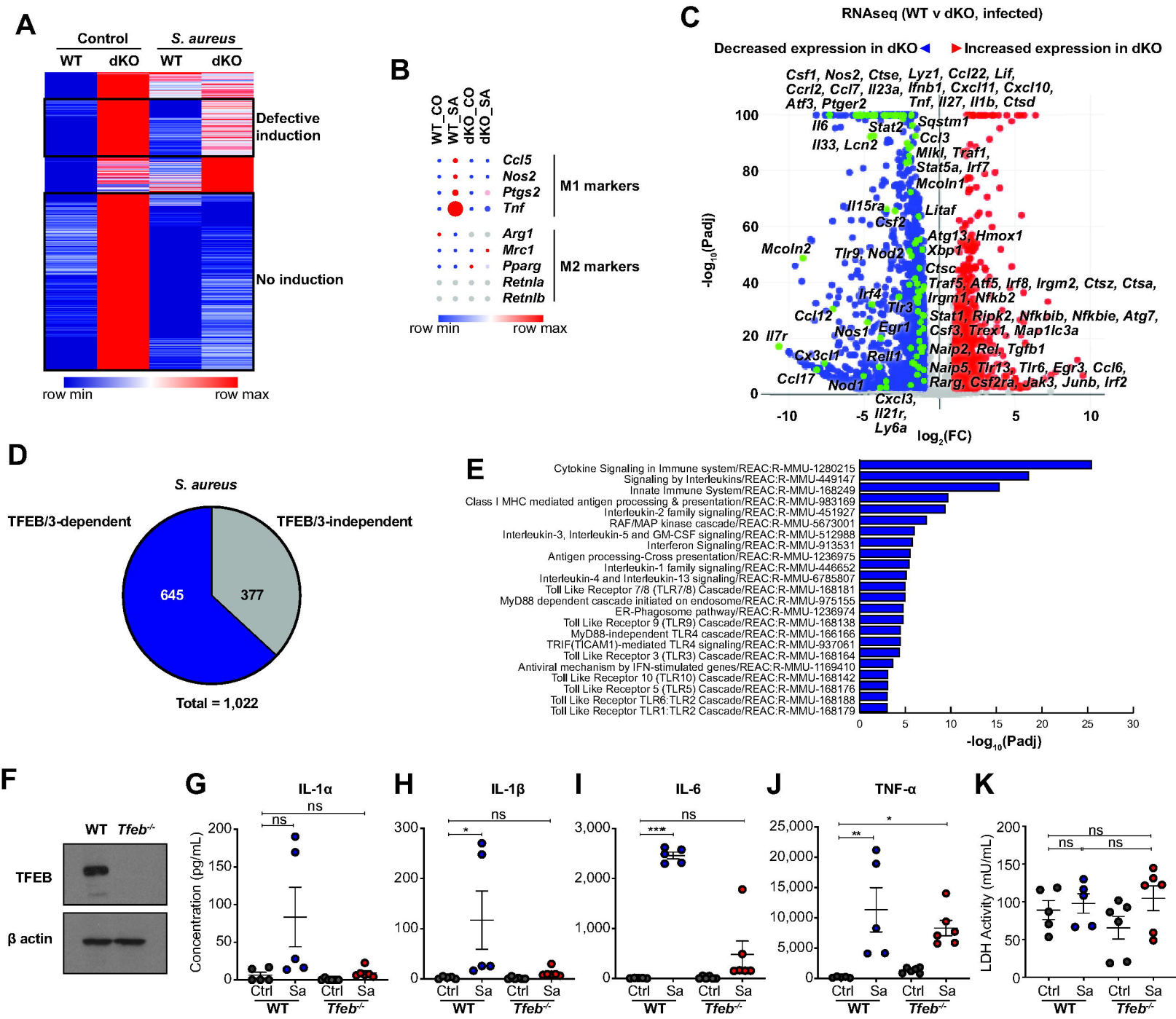
- 920 nary arterial smooth muscle. *Microvasc Res* **67**, 159–167 (2004).
- 921
- 922 35. Zhang, X. *et al.* MCOLN1 is a ROS sensor in lysosomes that regulates au-  
923 tophagy. *Nat Commun* **7**, 12109 (2016).
- 924
- 925 36. DeLeo, F., Allen, L., Apicella, M. & Nauseef, W. NADPH oxidase activation  
926 and assembly during phagocytosis. *J Immunol Baltim Md 1950* **163**, 6732–40  
927 (1999).
- 928
- 929 37. Slauch, J. M. How does the oxidative burst of macrophages kill bacteria? Still  
930 an open question. *Mol Microbiol* **80**, 580–583 (2011).
- 931
- 932 38. Marks, D. L. *et al.* Role of protein kinase d in Golgi exit and lysosomal target-  
933 ing of the transmembrane protein, Mcoln1. *Traffic* **13**, 565–575 (2012).
- 934
- 935 39. Park, D.-R., Nam, T.-S., Kim, Y.-W., Bae, Y. & Kim, U.-H. Oxidative activation  
936 of type III CD38 by NADPH oxidase–derived hydrogen peroxide in Ca<sup>2+</sup> signal-  
937 ing. *Faseb J* fj.201800235R (2018). doi:10.1096/fj.201800235r
- 938
- 939 40. Xu, M. *et al.* Contribution of NADPH Oxidase to Membrane CD38 Internaliza-  
940 tion and Activation in Coronary Arterial Myocytes. *Plos One* **8**, e71212 (2013).
- 941
- 942 41. Brady, O. A., Martina, J. A. & Puertollano, R. Emerging roles for TFEB in the

- 943 immune response and inflammation. *Autophagy* **14**, 1–9 (2017).
- 944
- 945 42. Vural, A. *et al.* Activator of G-Protein Signaling 3–Induced Lysosomal Bio-  
946 genesis Limits Macrophage Intracellular Bacterial Infection. *J Immunol* **196**, 846–  
947 856 (2016).
- 948
- 949 43. Singh, N. *et al.* Antimycobacterial effect of IFNG (interferon gamma)-induced  
950 autophagy depends on HMOX1 (heme oxygenase 1)-mediated increase in intra-  
951 cellular calcium levels and modulation of PPP3/calcineurin-TFEB (transcription  
952 factor EB) axis. *Autophagy* **14**, 1–57 (2018).
- 953
- 954 44. Ouimet, M. *et al.* Mycobacterium tuberculosis induces the miR-33 locus to  
955 reprogram autophagy and host lipid metabolism. *Nat Immunol* **17**, 677–686  
956 (2016).
- 957
- 958 45. Evans, T. D., Jeong, S.-J., Zhang, X., Sergin, I. & Razani, B. TFEB and tre-  
959 halose drive the macrophage autophagy-lysosome system to protect against  
960 atherosclerosis. *Autophagy* **14**, 1–7 (2018).
- 961
- 962 46. Sergin, I. *et al.* Exploiting macrophage autophagy-lysosomal biogenesis as a  
963 therapy for atherosclerosis. *Nat Commun* **8**, ncomms15750 (2017).
- 964
- 965 47. Emanuel, R. *et al.* Induction of Lysosomal Biogenesis in Atherosclerotic Mac-

966 rophages Can Rescue Lipid-Induced Lysosomal Dysfunction and Downstream  
967 Sequelae. *Arteriosclerosis Thrombosis Vasc Biology* **34**, 1942–1952 (2014).  
968  
969 48. Blasi, E., Radzioch, D., Merletti, L. & Varesio, L. Generation of macrophage  
970 cell line from fresh bone marrow cells with a myc/raf recombinant retrovirus.  
971 *Cancer Biochem Bioph* **10**, 303–17 (1989).  
972

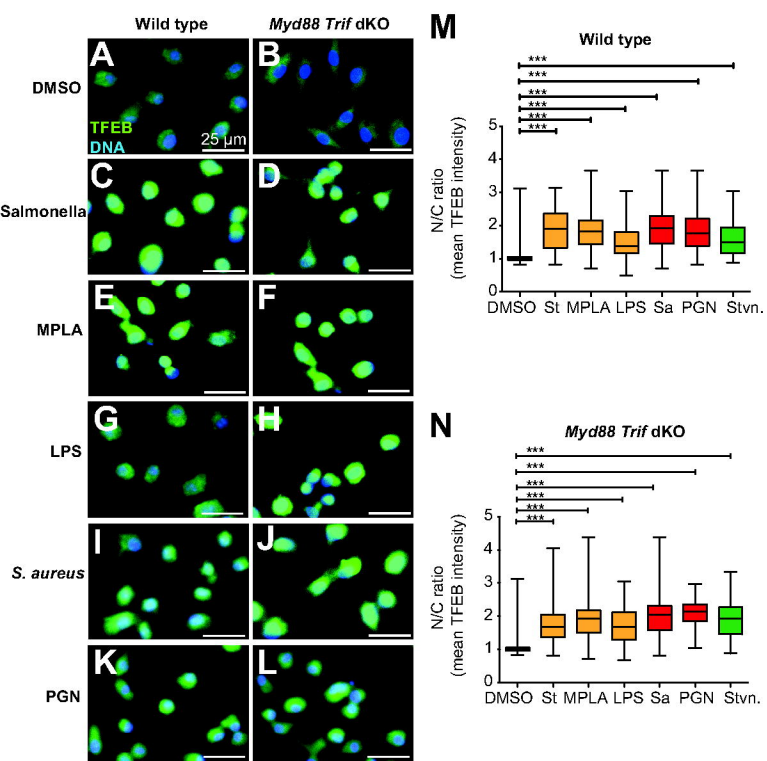


Najibi et al - FIGURE 2

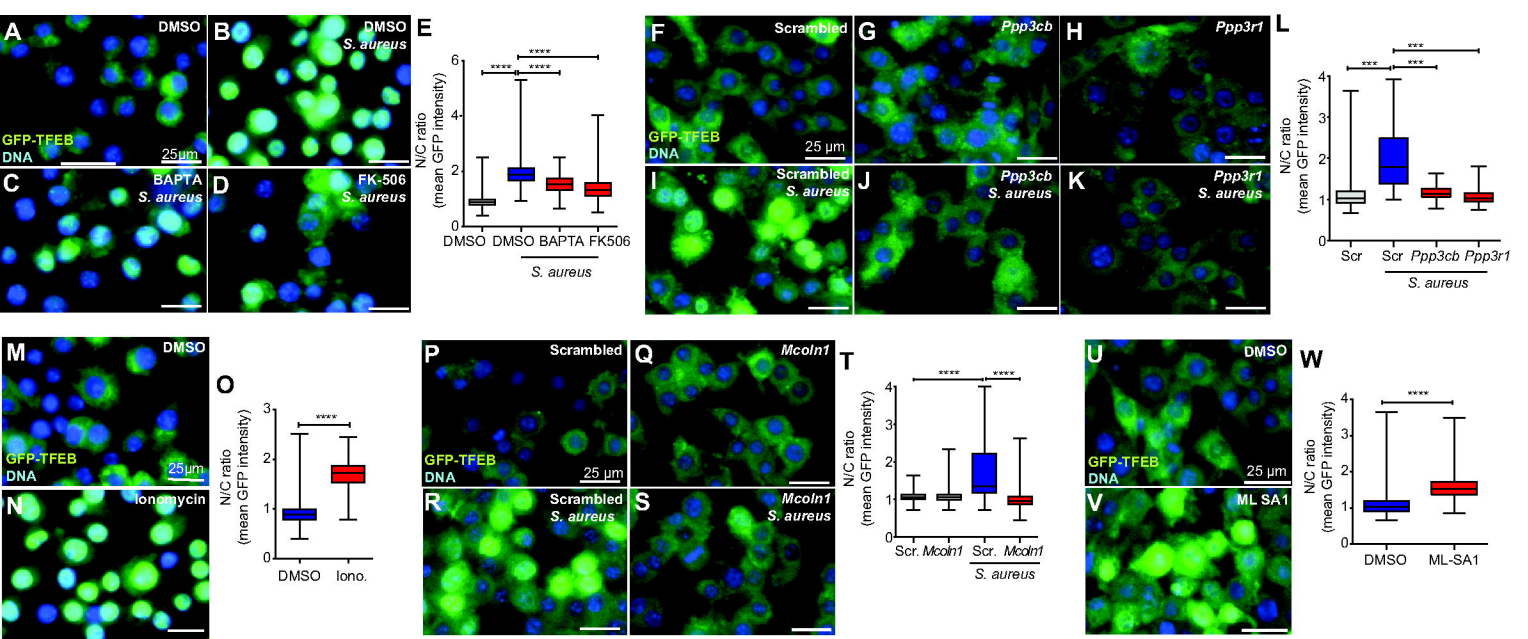




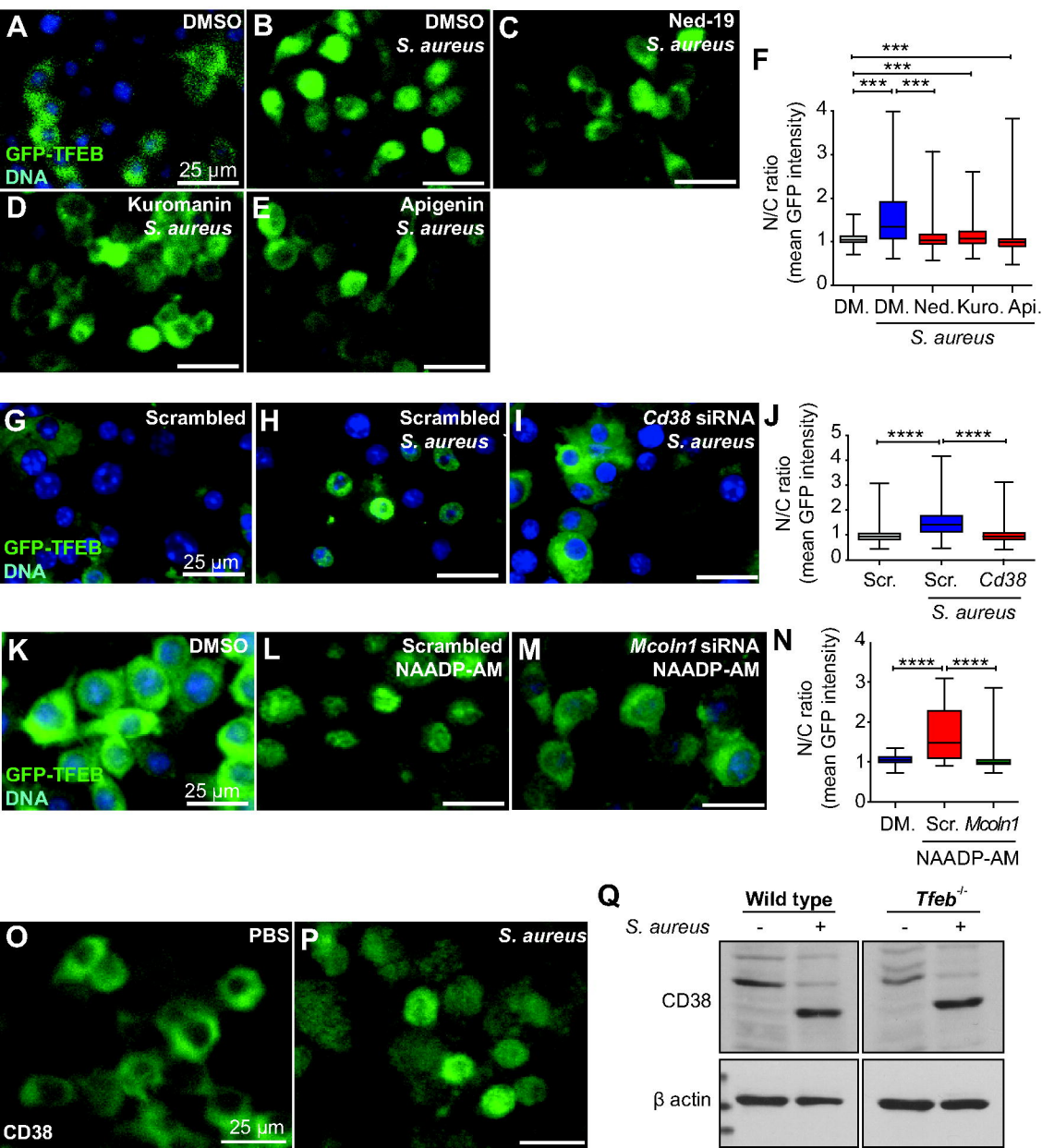
Najibi et al - FIGURE 3



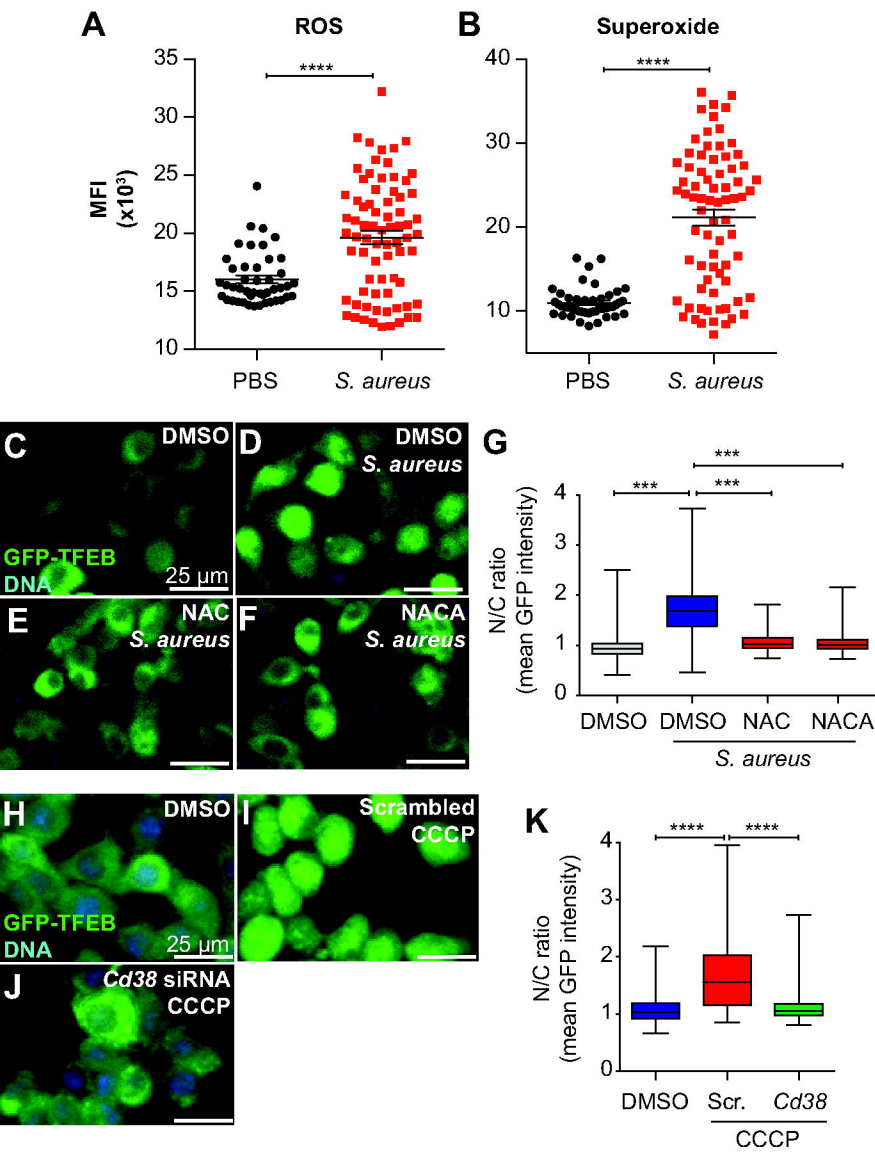
## Najibi et al - FIGURE 4



Najibi et al \_ FIGURE 5



## Najibi et al - FIGURE 6



Najibi et al - FIGURE 7

